POLITECNICO DI TORINO
Repository ISTITUZIONALE

The urban heat island of the Metropolitan City of Turin. Strategies for a sustainable urban planning

(Article begins on next page)

04 August 2020

THE URBAN HEAT ISLAND OF THE METROPOLITAN CITY OF TURIN. STRATEGIES FOR A SUSTAINABLE URBAN PLANNING

[a,#] **Guglielmina Mutani,** [a] **Valentina Cristino,** [a] **Martina Bullita**

[a]*Department of Energy, Politecnico di Torino, corso Duca degli Abruzzi 24, 10129 Torino (IT)*
(www.polito.it)
[#]*Corresponding Author: guglielmina.mutani@polito.it, +39 0110904528*

ABSTRACT

Globally, the world population living in cities is increasing and then the sustainability and liveability of urban spaces are rising the attention of the scientific community mainly in term of warming increase and health risk. In this work, the microclimate of outdoor spaces is investigated considering the different outdoor air temperatures registered by various weather stations in the city of Turin (Italy) and its surroundings with 12 municipalities. The air temperature variations are correlated with the built urban morphology, the solar exposure of urban spaces, the albedo coefficients of outdoor surfaces and other variables as the percentage of vegetation and water, the distance from the town centre and the Land Surface Temperature. With a multiple linear regression analysis the air temperatures have been correlated with the urban variables to obtain a simple model for the prediction of the average monthly air temperature in the Metropolitan City of Turin. This model can be used to understand the different microclimates within Turin and between the urban and the rural areas, and to evaluate the most influential variables on the air temperature variations. The resulted models could help urban planners to predict the microclimate in new districts, but also in the existent ones, as a function of the urban form and of the outdoor materials chosen to mitigate the UHI phenomenon.

KEYWORDS

UHI, microclimate, linear regression model, LST, albedo, NDVI, satellite images, sustainable urban planning.

1. INTRODUCTION

The consequences of global warming are now evident in our cities where concrete, asphalt, air pollution and anthropic activities cause temperatures up to 10°C higher than those in the surroundings or rural areas. This phenomenon in Climatology is named Urban Heat Island, referring to a urban area warmer than the surrounding suburbs [1]. Continued urbanization estimates that in 2050 the European population living in the city will be just over 80% resulting in increased risk for pollution, comfort, people health and consumption of fossil energy resources [2]. The UHI is also characterized by space-time variations within a city causing thermal discomfort and an increase of energy demand in summertime [3, 4].

The development of new megalopolis and the expansion of existing cities will increase the UHI phenomenon especially if this development is combined with the construction of new tall buildings, without the appropriate ventilation in

urban canyons and the with the use of waterproof materials with high absorption of solar irradiation [5]. Then, the control of the microclimate in urban environment becomes very important as it can contribute to a better liveability of the outdoor and indoor spaces [6, 7].

The analysis conducted in this work starts from previous researches about the influence of different materials used for outdoor urban spaces [8, 9], urban morphology [10] and Urban Heat Island [11], on air temperature variations in the urban environments. The results of these researches show clearly that in the city of Turin, the anthropic activities cause a typical UHI but with lower air temperatures near the parks and the rivers sides and higher temperatures in the high-density and industrial zones [12].

In this work, the above results were analysed on a larger territory around the city of Turin. More weather stations, different satellite images and additional indicators were investigated to implement the model for the prediction of air temperature variations (i.e. urban variables, solar exposure, albedo, the presence of vegetation and water and the distance from the town centre).

In the first part of this work, the state of art and literature review are treated. The second part is dedicated to the presentation of the case study and the evaluation of various factors influencing the air temperature gradients in the urban context. Then the in the last parts, the linear regression models are presented with a discussion on the results.

The main objective of this work was to find a compensative method with a simplified tool based on a multiple linear regression for a sustainable urban planning.

2. LITERATURE REVIEW

First studies and publications on UHI date back to the early 1990s and the UHI is a phenomenon that is recognized and studied globally. Currently urbanization, anthropic activities and the use of outdoor materials are the major-influence factors of climate change, although urban areas are a small portion of the Earth's surface [13]. The most notable consequence is the UHI, closely related to the air quality, overheating and population health problems. The magnitude or intensity of the UHI is related to the size of the city, but the UHI does not appear only in the big cities. The homogeneity of the development of the UHI is the result of an increasingly concentrated urban structure and its connections with suburban areas [14, 15, 16]. The highest temperatures are generally in the centre of a heat island often corresponding to downtown [14]. By classifying the warmer and the main emissive source in a city, primarily there is the most densely built area, followed by commercial and industrial spaces; while, lower temperatures can be registered in the agricultural, hilly and forest land [12].

Different types of UHI, also known as AUHI Atmospheric Urban Heat Island, can be find in literature (in Figure 1). Indeed, the UHI can be further classified in BLUHI (Boundary Layer Urban Heat Island) and CLUHI (Canopy Layer Urban Heat Island) depending on the height considered; the BLUHI and the CLUHI consider respectively the layer above and below the average height of the buildings. The CLUHI considers the layer below the average height of the buildings, where heat stagnates due to urban morphology and where people discomfort can be perceived [17].

In recent years, the UHI have been monitored, also at territorial scale with satellites and aerial platforms by the remote sensing. The main feature of remote sensing is the multi-spectrality with the possibility of simultaneously taking different images (of the same portion of territory) in different bands of the electromagnetic spectrum. Usually, the visible (VNIR) and the thermal infrared (TIR) portion of the spectrum are recorded by remote sensing; TIR represents the thermal energy emitted by the ground and then corresponds to its emissivity.
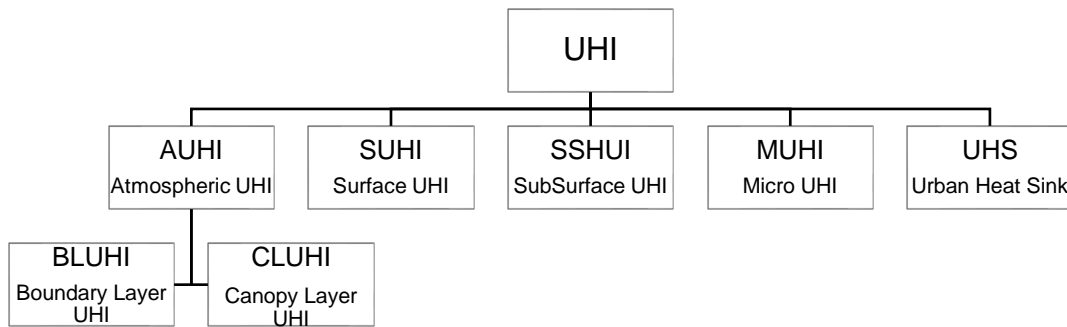

Figure 1. Types of UHI.

Table 1. State of art synthesis.

	YEAR	STUDY AREA	UHI	UHII	SUHI	MUHI	LST	LULC	NDVI	A	BD	BF	H/W	S	W	GIS
										URBAN VARIABLES				DATA		
[13]	2004	Indianapolis	●					●						●		
[18]	2007	Singapore	●					●						●		●
[15]	2009	Greece	●	●			●								●	
[16]	2010	World	●										●			
[3]	2011	Europe			●		●							●		
[30]	2011	Budapest	●				●							●	●	
[14]	2013	Shanghai	●				●								●	●
[19]	2014	Phoenix									●	●		●	●	
[24]	2014	India	●	●									●	●		
[2]	2015	Rotterdam	●							●				●		
[26]	2015	China	●				●	●	●					●	●	
[5]	2015	Saudi Arabia	●							●			●	●		
[9]	2015	Chicago	●							●				●		
[8]	2015	Turin	●								●	●				●
[6]	2015	World	●	●						●				●		
[4]	2015	Singapore	●									●	●			
[10]	2015	Italy	●				●			●	●	●	●	●	●	●
[11]	2015	Italy	●				●			●	●	●	●	●	●	●
[7]	2016	Italy	●							●	●	●	●	●		
[12]	2016	Italy	●							●	●	●	●	●		
[23]	2016	Vienna	●							●	●	●	●	●		
[1]	2016	Chile										●				●
[27]	2016	Dhaka											●			
[17]	2017	Beijing	●	●										●	●	●
[20]	2017	South America	●							●					●	●
[21]	2017	Perugia	●							●					●	
[31]	2017	Hangzhou, China	●		●		●			●				●	●	

Legend:

UHI = Urban Heat Island	LST = Land Surface Temperature
UHII = Urban Heat Island Intensity	LULC = Land Use Land Cover
SUHI = Surface Urban Heat Island	NDVI = Normalized Difference Vegetation Index
MUHI = Micro Urban Heat Island	NDWI = Normalize Difference Water Index
A = Albedo	H/W = Height/Width or Buildings Aspect Ratio
BD = Building Density	S = Satellite data
BF = Building Form	W = Weather data

The Albedo is one of the indicators that can be calculated by the remote sensing images. Albedo is the percentage of solar incident irradiation reflected by a surface, and is an intrinsic characteristic of the materials; in fact, a material such as asphalt, with very-low albedo values, tends to store and absorb more the incident solar irradiation, reaching high surface temperatures. Also, the presence of vegetation with the Normalized Difference Vegetation Index (NDVI) can be measured by remote sensing images with the difference between NIR (which vegetation reflects) and RED light (which vegetation absorbs).

With a GIS tool (Geographic Information Systems) it is possible to create and process the remote sensing images to study and to map the UHI taking into account all characteristics of the built environment ([1], [8], [14], [17], [18], [19], [20]). The classic indicator for describing an UHI is the difference between urban and rural temperatures and its intensity can be evaluated by minimum, average and maximum air temperatures [21]. To measure the intensity of the heat island, satellite data were also used to analyze temporal changes such as the Land Surface Temperature (LST) considering the development of the built-up areas and the decrease of the green zones. The results of this analysis may guide and plan the optimization of the land use and the choice of the most favourable land coverage.

Table 1 shows a synthesis of the state of art on UHI reporting the year and the area of the analysis, the variables involved, type of data (satellite or weather) and if the study used a GIS tool. The literature analysed concerned mainly studies on UHI (85%), considering the LST (26%), the A (44%) and the H/W (41%) with weather data (74%); only the 33% of the analysed literature used a GIS tool.

## 2.1. Study area: the case study of Turin

Turin is the fourth Italian city for population with almost one million inhabitants in the urban area and two million including the metropolitan area with a population density of about 6,800 inh/km^2. It is located in north-west part of Italy with a continental humid temperate climate but, since the nineties onwards, its weather has undergone a progressive warming with an increase of human health risks [22].

In this study, the territory of Turin was divided in 8 districts and in census sections corresponding to blocks of buildings dimensions. This analysis was extended to the following municipalities near Turin in which weather data were available: Brandizzo, Candiolo, Caselle, Chieri, Grugliasco, Moncalieri, Nichelino, Pecetto, Pino Torinese, Rivoli and Venaria Reale.

To evaluate the UHI phenomenon, air temperatures variations between the high-density urban context and the peripheries were analysed through temperature series of the past decade. A GIS-based method was used to calculate the various parameters influencing the air temperature variation.

In Figure 2 the weather stations considered in this study were represented and in Table 2 their main characteristics are reported with the distinction in urban and rural weather stations. Table 2 shows that, in the urban context, 4 weather stations (Giardini Reali, Politecnico, Università di Torino and via della Consolata) are near the centre of Turin; the other 5 weather stations are in the in the periphery of Turin. The rural weather stations have a variable distance from the centre of Turin from 5 to 17 km and two weather stations have higher

4

altitudes (Bric della Croce and Pino Torinese) and this can influence the UHI effects.
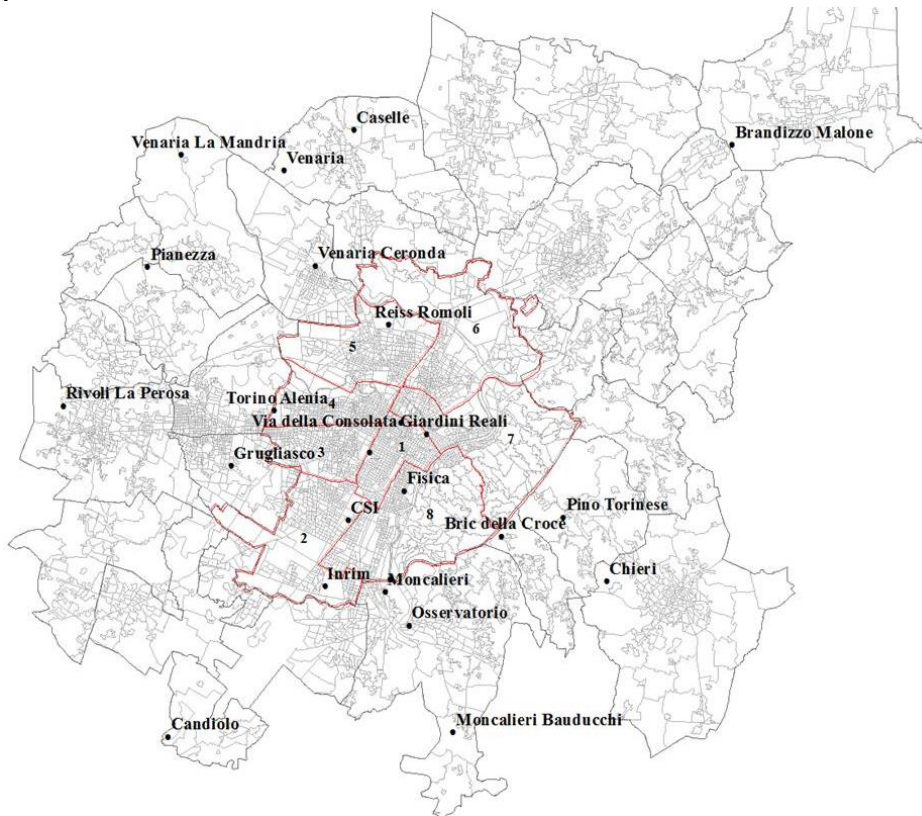
Figure 2. Relative location of the weather stations in Turin and near Turin.

Table 2. Weather Stations characteristics.

NAME	ARPA ID	MUNICIPALITY	LAT. N	LONG. E	Dst	CS	Alt$_{asl}$ [m]	D [Km]	Working from
URBAN WEATHERS STATIONS									
CSI		Torino	45,038331	7,651130	2	2166	270	3.814	2015
Giardini Reali	446	Torino	45,071702	7,691890	1	66	239	0.123	2004
INRIM		Torino	45,014047	7,639484	2	3096	242	6.069	2009
Reiss Romoli	S3869	Torino	45,112508	7,670910	5	3542	270	4.454	2003
Politecnico		Torino	45,064435	7,662004	1	797	233	1.316	2010
Torino Alenia	S4294	Torino	45,079646	7,610725	4	2414	320	5.173	2005
Università		Torino	45,050272	7,680429	8	868	254	1.737	2004
Vallere Smat	249	Torino	45,016980	7,673897	8	2295	239	4.096	2001
Via della Consolata	S3447	Torino	45,075930	7,678352	1	14	290	0.484	2003
RURAL WEATHER STATIONS									
Brandizzo Malone	373	Brandizzo	45,182019	7,851905		90	192	17.525	2005
Bric della Croce	16061	Pecetto Torinese	45,033850	7,732461		0	710	5.170	1954
Candiolo		Candiolo	44,956527	7,557674		17	245	15.222	2000
Caselle	S2896	Caselle Torinese	45,185429	7,650859		56	300	12.150	2003
Chieri		Chieri	45,017589	7,788666		177	357	9.047	2000
Grugliasco	144	Grugliasco	45,058599	7,588589		275	290	6.829	1987
Moncalieri	126	Moncalieri	45,012172	7,671533		216	290	5.565	2000
Moncalieri Bauducchi	273	Moncalieri	44,960107	7,708579		205	226	11.206	1993
Osservatorio		Moncalieri	44,999904	7,684481		2	287	6.925	-
Pianezza		Pianezza	45,132651	7,542330		28	319	11.026	1987
Pino Torinese	120	Pino Torinese	45,041336	7,765158		8	619	6.720	1988
Rivoli La Perosa	S3948	Rivoli	45,079869	7,498911		265	362	12.843	2004
Venaria La Mandria	S4587	Druento	45,174956	7,559208		26	337	13.465	2006
Venaria Ceronda	256	Venaria	45,134220	7,631300		2	253	7.881	1997
Venaria	130	Caselle Torinese	45,169695	7,613889		60	260	11.167	1987
Legend: Dst **=** District of Turin Alt$_{asl}$ **=** Altitude above sea level				CS **=** Census Section D [Km] = distance in kilometres from the town center.					

3. MATERIAL AND METHODS

The methodology proposed in this study can be explained through the following steps:
1. Climate data collection of public and private weather stations in urban and suburban areas for a long time-period with the definition of a typical year.
2. Data collection from national, regional and municipal databases to describe the case-study territory with the definition of geographic coordinates for a spatial data distribution and representation of the built environment.
3. Definition and numerical evaluation of the environmental variables that influence microclimate variations (with the support of satellite images).
4. Evaluation of a simple model to describe the influence of environmental variables on air temperature variation with a multiple linear regression.

In step 3, the most influential variables on the air temperatures were evaluated considering the higher correlation factors. For example, since BCR and MOS were among the most influential, it was decided to exclude BD, BH and BO related to them, but less influential.

Then, in step 4, the linear regression models of the monthly air temperature were performed considering the most influential available variables on the whole territory. In this model the air temperature is the dependent variable, T_{air}, that can be evaluated as a linear function of the "n" other independent variables X [7, 12]:

$$T_{air} = I + \alpha_1 \cdot X_1 + \alpha_2 \cdot X_2 + \cdots + \alpha_n \cdot X_n + \varepsilon \tag{1}$$

where:

I   is the intercept;

α_1- α_n are coefficients that can estimate the influence of a variable on the air temperature; α has a negative sign when the air temperature decreases if its variable increases and a positive sign when the air temperature increases when its variable increases.

X   are the independent variables.

ε is the error associated to the model.

Four different types of variables were used to define the model [21, 23]:
- real data or with normalized data; normalized variables have an average value equal to 0.5 so that all variables have the same average value and don't have different units of measure; then the α coefficients are the weight with which the variable influences T_{air};
- real classes or normalized classes; the following variables were subdivided in classes depending from the: distance from the city centre (from 0 <2 km; 1 <6 km; 2 <10 km; to 3), presence of vegetation (from 0 to 1 without or with vegetation) and altitude (1 with +1-20 m, 2 with +20-50 m and 3 with +50-100); normalized classes have an average value equal to 0.5.

In this work, the more interesting models with normalized variables are reported.

Mainly, the morphology of the built environment was evaluated through geometrical variables evaluated with a GIS tool, while the features of the materials characterizing the territory were elaborated through georeferenced satellite images.

The results of the linear regression model of air temperature were also compared with the Land Surface Temperature (LST) registered by satellite images. All analyses consider a territorial unit equal to block of buildings area.

3.1. Climate data evaluation and definition of the typical year

Climate data were obtained by public authorities and private companies through online portals or direct requests. In Piedmont Region, most of weather databases are managed by ARPA (Regional Agency for the Protection of the Environment) and by the RAM (Agro-Meteorological Network) [24]. To estimate the UHI phenomenon, the hourly and monthly air temperatures of the last decade (2005-2016) have been collected and represented using an Excel spreadsheet to evaluate their trends and to find their monthly typical trend on this period of time [18, 25].
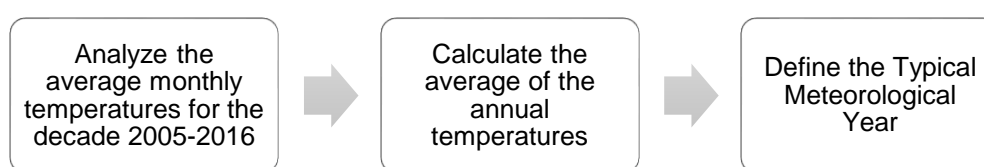
Figure 3.First step to evaluate the air temperature trends and the typical year.

In the territory near Turin and for these 12 years from 2005 to 2016, the average air temperature was about 13.98°C; then the year 2012 was chosen as a typical one with an average air temperature of 13.97 °C. In urban context, from these data can also be observed that in 12 years, the on average air temperatures increase of +3.4 °C in February and of +2.0 °C in August.

Table 3. Typical Meteorological Year 2012.

	Jan	Feb	Mar	Apr	May	Jun	Jul	Aug	Sep	Oct	Nov	Dec	Tavg
Vallere Smat	1.80	-0.40	11.30	12.00	17.20	22.60	23.90	24.60	18.30	13.40	8.30	1.80	12.90
Reiss Romoli	3.50	2.10	13.10	12.10	17.90	23.10	24.50	25.00	19.40	14.40	9.30	2.90	13.94
Via Consolata	4.40	2.70	13.60	12.60	18.50	23.70	25.30	25.90	19.90	15.00	10.00	3.90	14.63
Giardini Reali	2.80	1.70	12.20	12.10	17.70	22.80	24.40	25.10	18.80	13.80	8.80	2.30	13.54
Torino Alenia	3.60	1.60	12.90	11.90	17.60	22.90	24.20	24.90	19.10	14.20	9.20	3.20	13.78
Inrim	1.90	1.31	11.95	12.25	17.70	23.06	24.53	25.12	19.15	13.77	8.62	2.32	13.47
Politecnico	4.54	2.81	13.95	12.99	18.70	23.94	25.53	26.31	19.56	15.53	10.56	4.60	14.92
Università	3.75	2.80	13.40	12.80	18.50	23.60	25.10	25.60	19.90	15.20	10.30	4.20	14.60
CSI	4.45	2.73	13.74	12.73	18.69	23.95	25.56	26.17	20.11	15.16	10.10	3.94	14.78
Moncalieri Baudu.	0.80	-2.10	10.70	12.00	17.60	22.70	23.90	24.00	18.10	13.10	-	1.10	12.90
Moncalieri Osser.	3.06	0.71	13.09	12.88	19.04	24.58	26.35	26.83	19.98	14.82	9.18	2.75	14.44
Brandizzo Malone	1.20	-0.30	11.10	11.70	17.10	22.40	23.60	24.00	18.10	13.20	7.90	0.90	12.58
Caselle	2.20	0.70	11.80	11.50	17.20	22.60	24.20	24.90	18.80	13.80	8.30	1.60	13.13
Pino Torinese	4.50	1.80	11.90	9.80	16.00	21.10	22.80	23.60	17.60	13.00	8.30	3.30	12.81
Venaria Ceronda	1.40	-0.40	10.90	11.50	16.80	22.20	23.40	24.00	18.00	13.10	7.80	-	13.52
Venaria IMandria	1.40	-0.50	10.60	10.90	16.20	21.70	-	23.50	17.60	12.70	7.30	0.90	11.12
Bric della Croce	3.13	5.81	11.16	9.37	15.08	19.44	21.44	22.79	17.71	11.91	7.58	3.35	12.40
Rivoli la Perosa	2.90	0.40	12.00	11.60	17.30	23.20	24.50	25.20	18.80	13.50	8.60	2.50	13.38
Candiolo	1.09	-2.39	11.13	11.99	17.42	23.06	24.13	24.78	18.37	13.21	7.75	1.08	12.63
Chieri	3.41	1.29	12.28	11.54	16.90	22.19	22.48	23.03	17.68	13.41	8.95	3.13	13.02
Grugliasco	3.40	1.73	12.78	12.21	17.84	23.34	24.79	25.55	19.57	14.16	9.02	2.89	13.93
Moncalieri	1.38	-0.93	10.96	12.06	17.30	22.75	23.97	24.52	18.36	13.43	8.03	1.33	12.76
Pianezza	2.40	0.21	11.29	11.22	16.35	21.75	22.68	23.48	18.07	13.17	8.14	1.72	12.53
Venaria	2.90	1.06	12.28	11.85	17.30	22.69	23.83	24.61	18.82	13.99	8.72	2.36	13.36
Tavg mth	2.56	0.90	11.52	11.29	16.63	21.72	23.02	23.64	17.90	13.16	8.29	2.35	
TGavg	0.07	0.00	0.47	0.46	0.69	0.92	0.97	1.00	0.75	0.54	0.32	0.06	

In Table 3 were collected the monthly temperatures registered in the 2012 by all the active weather stations. This analysis shows differences between the air temperatures of the urban and suburban contexts. In the last rows, the lowest average monthly temperature is highlighted in blue (February) and the highest one in red (August). Between the urban weather stations, the one with the lower annual air temperature is Vallere Smat with 12.90°C because of its green environment with also the presence of Po river; within the rural weather stations, the coldest are Venaria La Mandria in a big park and Bric della Croce in the hillside at 710 m of altitude. With regard to the maximum annual average temperature, the warmest air temperature is recorded by Politecnico with 14.92°C in a high-density zone with about +2°C compared to the suburb areas.

From the average monthly temperatures $T_{avg,mth}$, the average Thermal Gradient (TG_{avg}) was obtained:

$$TG_{avg} = (T_{avg,mth} - T_{min})/(T_{max} - T_{min}). \qquad (2)$$

This variable, varying from 0 to 1, can be used in a model to evaluate monthly variations in a typical year (in the last row of Table 3).

3.2 Data collection of territory characteristics

To analyse the urban and rural morphology and to calculate the environmental variables, different databases and geospatial datasets have been acquired; in particular: the Technical Map of the Metropolitan City of Turin (CTP), the Municipal Technical Map for the City of Turin (CTC), and the BDTRE 2016 file-package from Piedmont Region geoportal). Other information about socio-economic data were obtained from the ISTAT 2011 census database.

To evaluate the type of material of the territory in urban and rural areas, satellite images have been used. Two different sources have been compared: the Landsat 8 images with an extension of 180 x 180 km (low resolution) and the ASTER images with an extension of 60 x 60 km (higher resolution). The satellite LANDSAT-8 OLI images have been acquired from the Earth Explorer website while the Aster images have been provided from CSI (Consortium for the Information System) of Piedmont Region. Aster images date back to 22nd July 2004 at 10.33 am because in the years later the SWIR sensor broke down. Then, the Landsat images for the comparison were chosen in days with similar air temperatures and with clear sky conditions (same and low cloud cover percentage); in this work, Landsat images refer to July 23rd 2013 at 10.19 am.

## 3.3. Urban parameters that influence the microclimate

As observed in literature, the microclimate variations are strongly influenced by the environmental context as the urban morphology, the solar exposition, the type of materials used in the outdoor spaces and the presence of vegetation and water [26, 27]. In this work, these characteristics have been evaluated with a GIS tool considering the block of building as a territorial unit for the urban context (with an area of 33.7 ha) and a larger area for the rural context (of about 340.3 ha: 583x583 m^2).

The following environmental variables, that influence the air temperature variations, were calculated with a GIS tool for each territorial unit:
- BCR - building coverage ratio [m^2/m^2], ratio between built area and the territorial unit area.

- H/W - aspect ratio or height to distance ratio [m/m], ratio between the height of buildings and their distance.
- H/H_{avg} - relative height of a building [m/m], ratio between the height of a building and the average height of the surrounding buildings.
- BD - building density $[m^3/m^2]$, ratio between the buildings volume and the territorial unit area.
- BH - buildings height [m], average height of buildings within the territorial unit.
- MOS - main orientation of the streets [-], prevalent orientation of streets and even consequently of buildings (BO); this value varies from 0.8 with orientation South-North to 1.3 East-West.
- Alt_{asl} – altitude above sea level [m]: the air temperature decreases with higher altitudes.
- D - distance from the city centre (the Roman quadrilateral area in Turin) [km] to consider the typical effect of the UHI: usually, with the increase of the distance from the city centre, a decrease in air temperature is observed.
- H_2O - the presence or the absence of water (respectively 1 or 0).

To evaluate the outdoor materials used in the outdoor spaces (characterized by the albedo coefficient) and the presence of vegetation (with the NDVI index varying from -1 to +1; low values correspond to arid areas of rock, sand, or snow while high values indicate tropical rainforests), satellite data derived from the Landsat-8 and the Aster images were utilized. These images were also used to evaluate the LST and all the satellite data were georeferenced with a GIS tool (Figure 4).
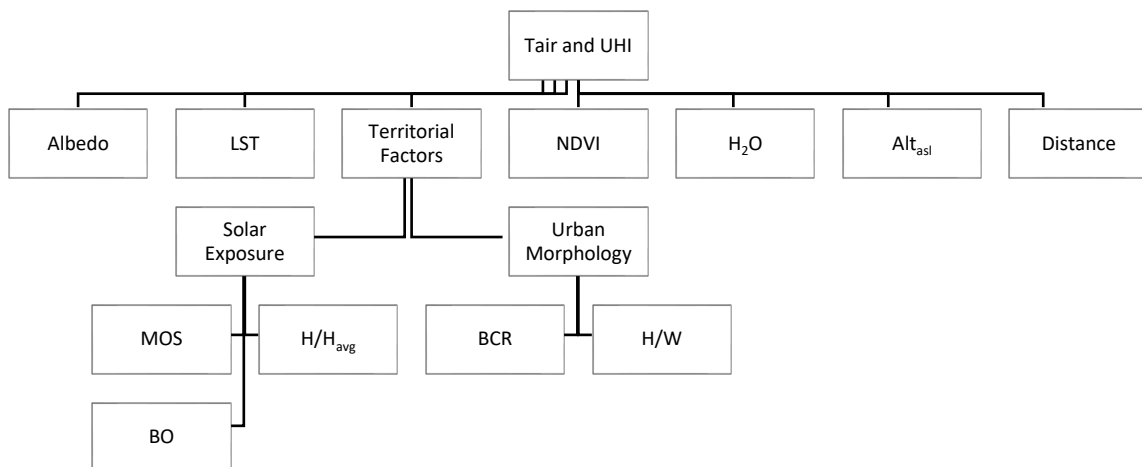
Figure 4. Parameters influencing the air temperature and the UHI.

Compared to Landsat 7, Landsat 8 installs also optional land imager (OLI) and thermal infrared (TIRS) sensors. Thanks to these sensors, the number of recording spectrum bands increases from 9 to 11 with the addition of an ultra-blue band at 0.43-0.45 µm and band 9 useful to evaluate the cloud cover at 1.36-1-38 µm. In addition, the TIR field is separated by band 10 called TIR1 at 10.60-11.19 µm, and band 11 called TIR2 at 11.50-12.51 µm. The goal of this satellite sensors is to be able to deliver higher resolution images both in visible and infrared compared to Landsat 7 with 16 instead of 8-bit.

To derive the albedo coefficients A, NDVI and LST, the algorithms of Liang ([28], [29]) have been used for Aster and Landsat-7 ETM+, considering the different fields of wavelength for Landsat-7 and Landsat-8 reported in Table 4.

Table 4. Spectral bands and spatial resolution comparison between Landsat-7 and Landsat-8 satellite images.

| Landsat-7 ETM+			Landsat-8 with OLI and TIRS Bands		
Band	**Spatial resolution**	**Wavelenght (μm)**	**Band**	**Spatial resolution**	**Wavelenght (μm)**
			1	30 m Coastal/Aerosol	0.435-0.451
1	30 m Blue	0.441-0.514	2	30 m Blue	0.452-0.512
2	30 m Green	0.519-0.601	3	30 m Green	0.533-0.590
3	30 m Red	0.631-0.692	4	30 m Red	0.636-0.673
4	30 m NIR	0.772-0.898	5	30 m NIR	0.851-0.879
5	30 m SWIR-1	1.547-1.749	6	30 m SWIR-1	1.566-1.651
6	60 m TIR	10.31-12.36	10	100 m TIR-1	10.60-11.19
			11	100 m TIR-2	11.50-12.51
7	30 m SWIR-2	2.064-2.345	7	30 m SWIR-2	2.107-2.294
8	15 m Pan	0.515-0.896	8	15 m Pan	0.503-0.676
			9	30 m Cirrus	1.363-1.384

4. RESULTS

In Table 5 the main variables have been calculated for the areas of the selected weather stations. In the high-density centre of Turin, it is possible to observe: in Figure 5 the high values of BCR, in Figure 6 the low values of albedo, in Figure 7 the low values of NDVI (absence of vegetation) and in Figure 8 the high values of LST. Vice versa in the suburb zones.

**Table 5**. Main urban variables in the weather stations' zones.

| Weather Station	BCR [m²/m²]	H/W [m/m]	H/H [m/m]	MOS [-]	A_{nir} Landsat [-]	A_{nir} Aster [-]	D [Km]	NDVI Landsat [-]	NDVI Aster [-]	H_2O [-]
Vallere Smat	0.14	0.34	0.81	1.01	0.21	0.27	4.096	0.56	0.43	1
Reiss Romoli	0.38	0.37	1.50	0.94	0.21	0.30	4.454	0.23	0.23	0
via Consolata	0.43	0.38	1.04	0.97	0.14	0.22	0.484	0.1	0.11	0
Giardini Reali	0.01	0.38	0.83	1.03	0.21	0.28	0.123	0.24	0.47	0
Alenia	0.36	0.59	1.89	1.03	0.20	0.26	5.173	0.22	0.22	0
Inrim	0.08	0.34	1.19	1.05	0.24	0.31	6.069	0.47	0.47	0
Politecnico	0.39	0.48	1.50	1.02	0.17	0.26	1.316	0.3	0.22	0
Università	0.47	0.22	1.14	0.99	0.16	0.23	1.737	0.16	0.24	0
Csi	0.17	0.83	2.14	1.04	0.20	0.28	3.814	0.33	0.33	0
Bauducchi	0.01	0.10	0.68	0.90	0.27	0.33	11.206	0.58	0.60	1
Osservatorio	0.65	0.27	1.76	0.93	0.20	0.28	6.925	0.25	0.25	0
Brandizzo	0.01	0.14	1.17	1.05	0.25	0.33	17.525	0.53	0.53	1
Caselle	0.29	0.12	0.83	0.94	0.29	0.36	12.150	0.6	0.60	1
Pino Torinese	0.12	0.20	1.09	0.98	0.26	0.33	6.720	0.58	0.60	0
Ceronda	0.13	0.24	1.41	0.87	0.19	0.25	7.881	0.32	0.32	1
Mandria	0.00	0.13	1.17	1.12	0.28	-	13.465	0.66	-	1
Bric Croce	0.09	0.22	1.23	0.97	0.29	0.33	5.170	0.7	0.70	1
Rivoli Perosa	0.01	0.16	1.02	1.07	0.27	-	12.843	0.6	-	1
Candiolo	0.01	0.09	1.34	0.97	0.29	0.34	15.222	0.51	0.51	1
Chieri	0.02	0.15	0.91	1.01	0.29	0.36	9.047	0.54	0.54	1
Grugliasco	0.17	0.10	0.81	0.70	0.25	0.33	6.829	0.4	0.40	0
Moncalieri	0.01	0.19	0.92	0.96	0.26	0.33	5.565	0.56	0.56	1
Pianezza	0.02	0.17	1.00	0.92	0.30	-	11.026	0.56	-	1
Venaria Caselle	0.02	0.23	1.15	0.97	0.29	0.35	11.167	0.63	0.63	1
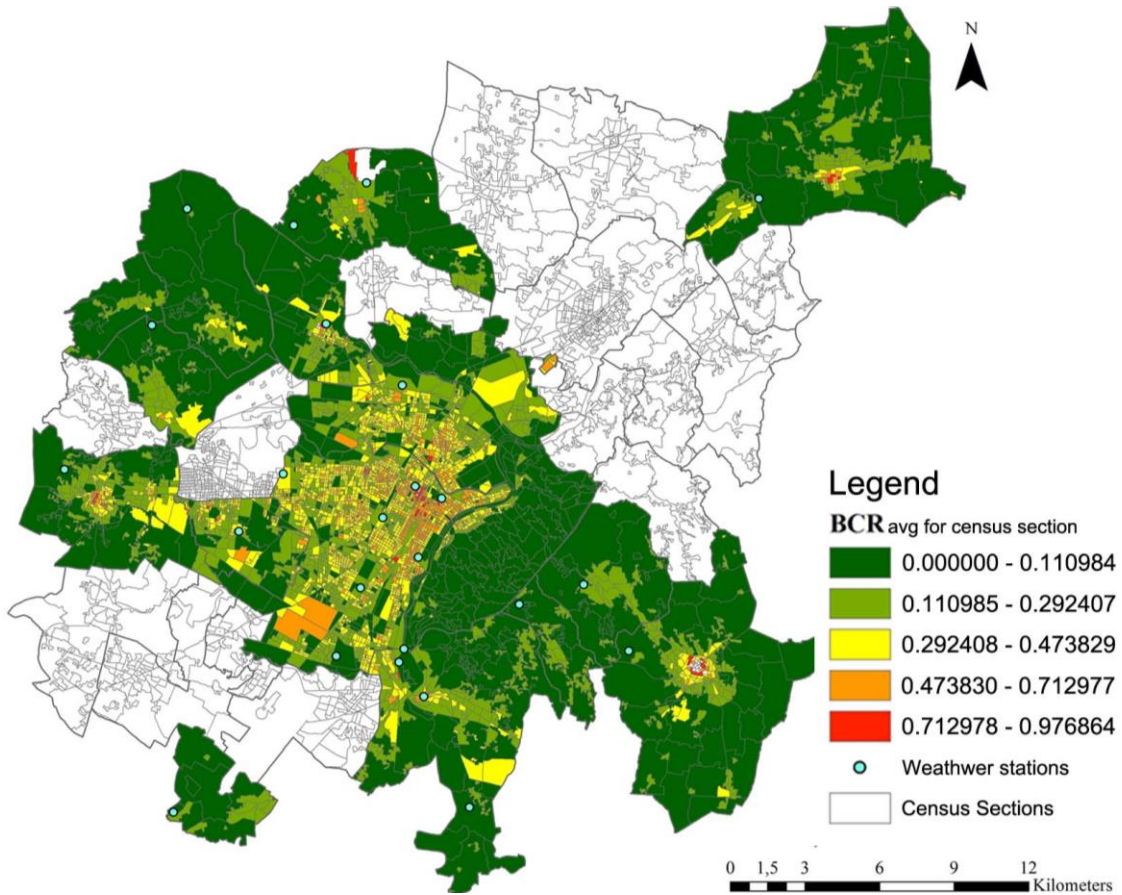
Figure 5. Map of the average BCR [m^2m^2] values for census section.
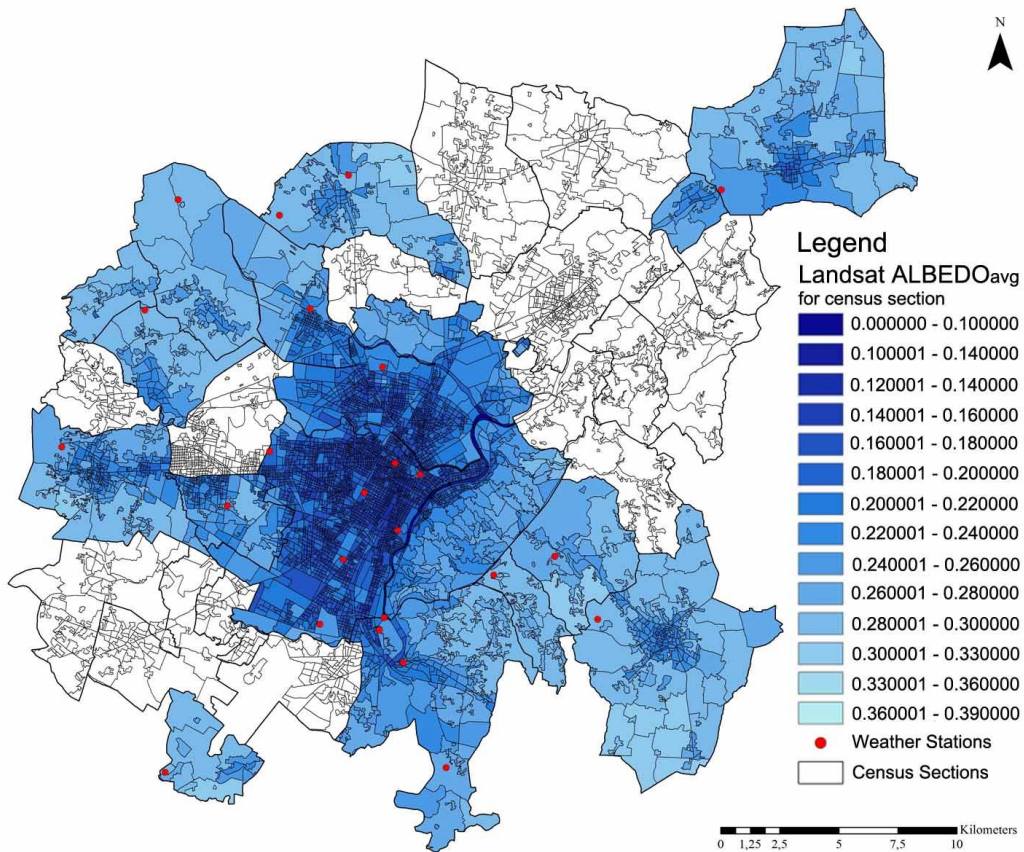
Figure 6. Map of the average Landsat Albedo (near-IR values).
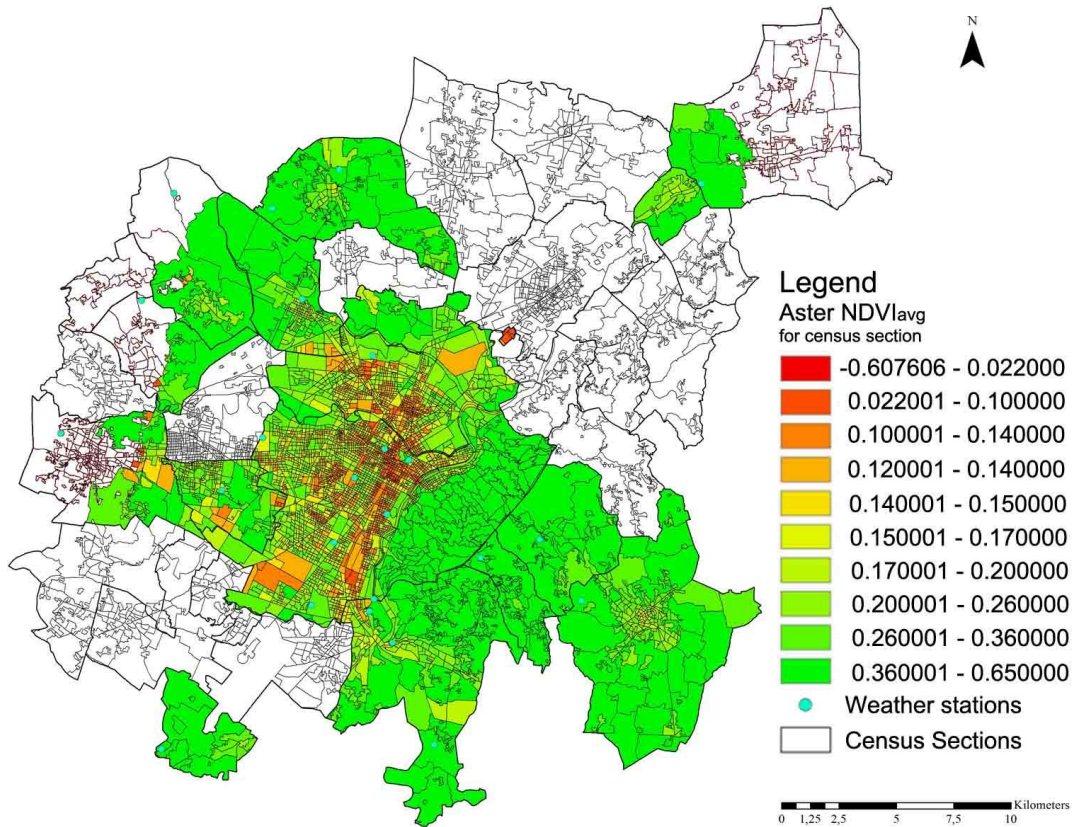
Figure 7. Map of the average Aster NDVI values for census section.
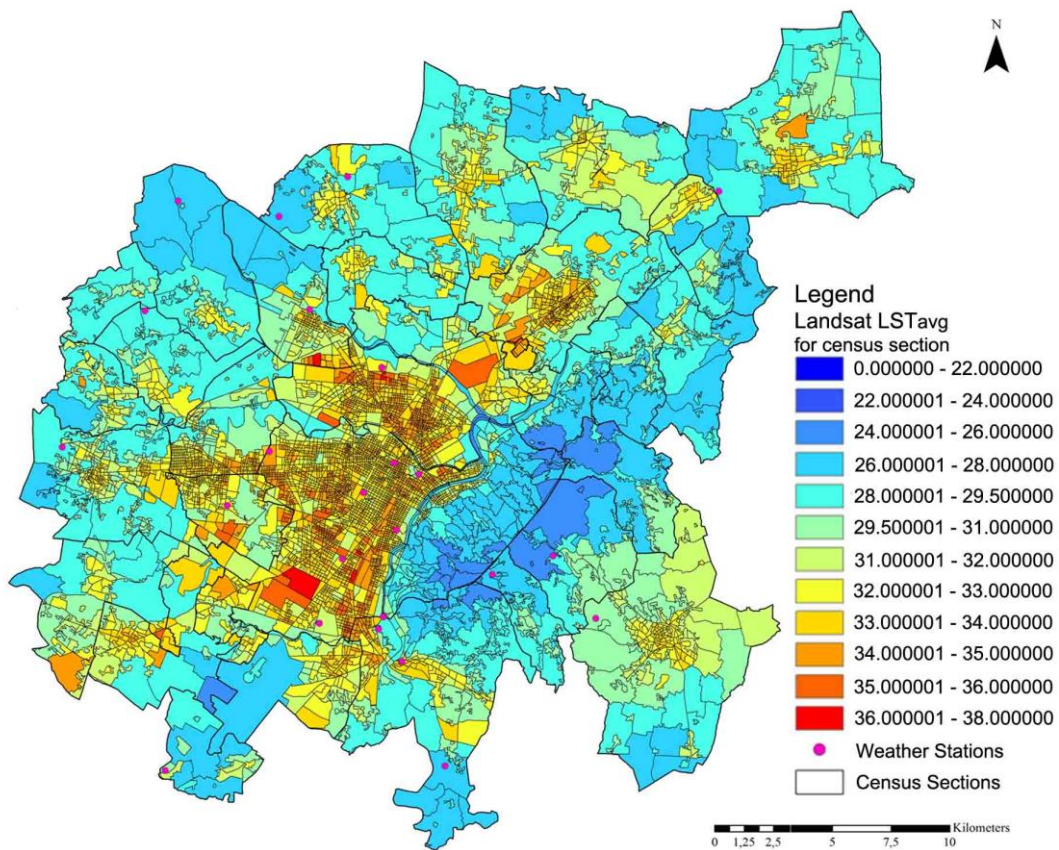
Figure 8. Map of the average Landsat LST (July 23rd 2013 at 10.19 am).

The main urban variables characterizing the surrounding environments, reported in Table 5, were normalized (with an average value of 0.5) and used to calculate the monthly air temperature with a linear regression model:

$$\boldsymbol{T_{air}} = I + (\alpha_1 \cdot BCR) + \left(\alpha_2 \cdot \frac{H}{W}\right) + \left(\alpha_3 \cdot \frac{H}{H_{avg}}\right) + (\alpha_4 \cdot MOS) + (\alpha_5 \cdot TG_{avg}) +$$
$$(\alpha_6 \cdot A) + (\alpha_7 \cdot D) + (\alpha_8 \cdot NDVI) + (\alpha_9 \cdot H_2O) + (\alpha_{10} \cdot Alt_{asl}) + \varepsilon. \tag{3}$$

Reducing the relative error between the calculated and measured air temperatures, multiple linear regression models have been evaluated. Starting from the results of past research [7, 12], in the multiple regression models were added more variables from A to Alt_{asl} in equation 3, determining the coefficients α reported in Table 6 (the intercept "I" was equal to zero).

Table 6. The coefficients α and the relative error ε for the multiple linear regression models.

|	Eq.	α1(BCR)	α2 (H/W)	α3 (MOS)	α4 (H/Hav)	α5 (TGav)	α6 (A)	α7 (D)	α8 (NDVI)	α9 (H20)	α10 (Alt)	ε %
Landsat	(4)	0.86	1.38	0.34	-0.95	24.08	0	-	-	-		7.3
	(5)	0.79	1.34	0.03	-0.48	24.22	-0.24	0	-	-		7.1
	(6)	0.69	1.21	1.99	-1.26	24.03	0	-0.99	-	-		6.9
	(7)	0.62	0.82	1.52	-0.53	24.16	0	0	-0.52	-0.45		6.7
	(8)	0.70	0.68	2.92	0.58	23.88	0	0	0.08	-0.47	1.51	6.4
Aster	(9)	0.97	1.44	0.33	-0.94	24.11	0	-	-	-	-	7.2
	(10)	0.90	1.31	0.23	-0.57	24.15	0	-0.10	-	-	-	6.9
	(11)	0.74	1.18	1.77	-0.99	24.17	0	0	-1.05	-	-	6.7
	(12)	0.68	0.64	1.68	-0.49	24.17	0	0	-0.43	-0.49	-	6.5
	(13)	0.78	0.68	2.88	0.55	23.99	0	0	0.07	-0.48	1.53	6.2

The best results, with the lower error between measured and calculated air temperature, were provided by equations 8 and 13 including all variables. This was predictable and it is realistic because it is well known that the altitude affects the air temperature and the urban heat island effect, as well as the distance from the centre of the main city and the presence of green and water. The relative error of the models was lower than 14% considering the 12 months; since the winter 2012 was quite cold with average monthly temperatures of about 0 °C, in the evaluation of the relative errors, the months of December, January and February were excluded, with maximum relative errors < 7%.

In Figures 9 and 10 the results about the spatial distribution of air temperatures calculated with equation 13 for the months of February and August is represented.

In order to verify the results and the consistency of the model, with the equations that gave the lower error (eq. 8 and 13), the air temperature computed by the model was also compared with the Land Surface Temperature (LST) [30]. LST influences indirectly the air temperature because the materials and outdoor surfaces absorb heat and solar irradiation and then exchange heat by convection with the air that that flows over them. The measure of LST can be obtained from satellite images and depends on the time in which the satellite image is captured. For ASTER, LST is calculated on July 22nd 2004 at 10.33 am, while for LANDSAT-8 on July 23rd 2013 at 10.19 am. To shift from the hourly to the daily LST, the time temperature distribution factor F(t) of Italian Standard UNI/TR 10349-2:2016 was applied to describe the hourly distribution of the air temperature between a minimum and a maximum in July.
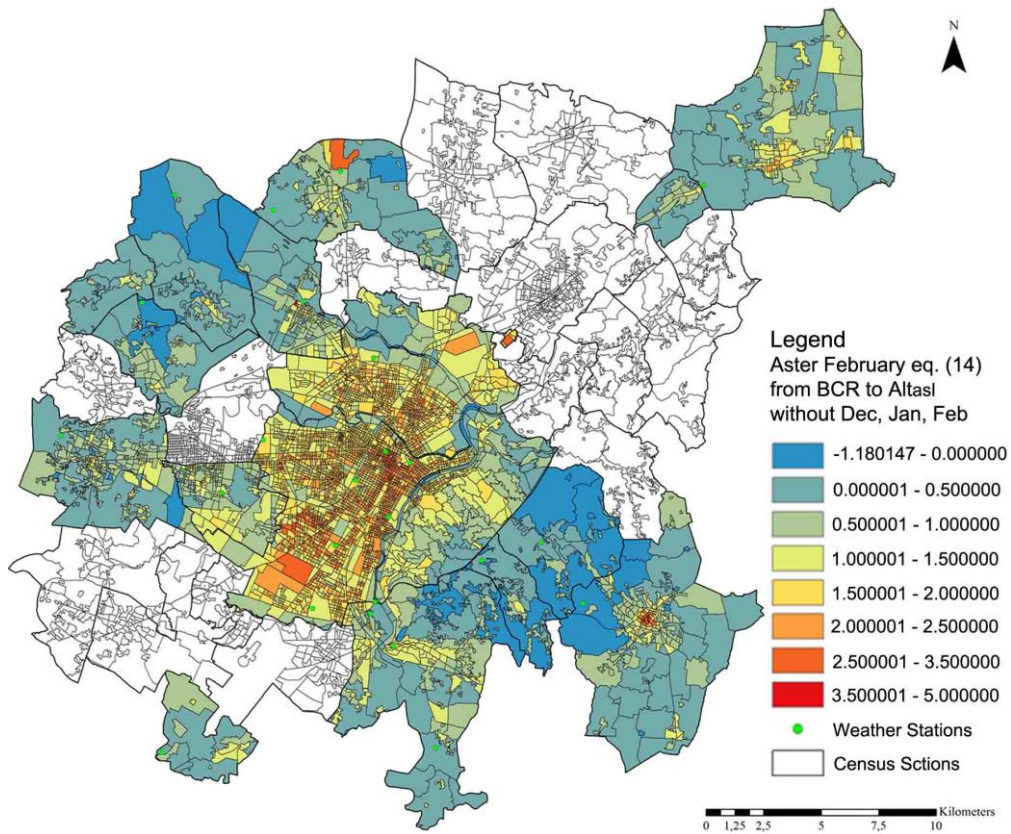
Figure 9. The air temperature calculated with equation 13 in February 2012.
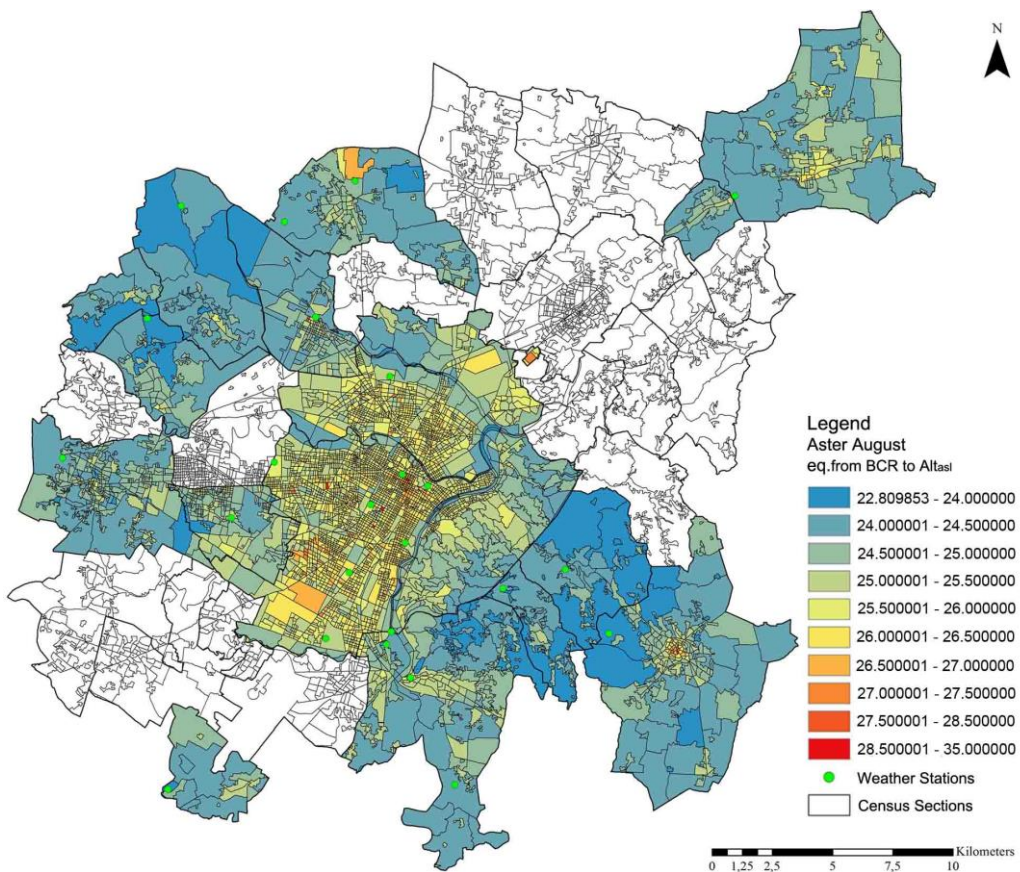
Figure 10. The air temperature calculated with equation 13 in August 2012.

14

With the daily LST, it was possible to determine a temperature gradient given by the difference between the daily LST and air temperature. The same procedure has been applied in urban and suburban contexts to map the differences between air temperature and LST and to highlight the urban heat island effect in the Metropolitan City of Turin.

The UHI effects was evaluated by temperature differences between urban and rural contexts through three indicators [31]:
1. The UHI-driven indicator "magnitude" (Q1) equal to the maximum temperature minus the average temperature;
2. The UHI-driven indicator "range" (Q2) equal to the difference between the maximum and the minimum daily temperature;
3. The land cover-driven indicator "urban-rural" (Q3) describes the difference between the daily temperature at urban (high-density area) and rural (low-density area) weather stations.

In this work, these three indicators were calculated over the period 2010-2016 for 12 weather stations with the daily average, maximum and minimum air temperatures; the results are reported in Table 7 considering the population density calculated through a buffer with a radius of 2.5 km around the weather stations.

For the urban weather stations, Q1 and Q2 are lower than the average value (in winter: 5.95-11.42 °C; in summer: 5.26-9.56 °C) because the average temperature in the urban context is higher.

The cover-driven indicator "urban-rural" Q3 was calculated with the difference of the average temperature in urban and rural context with 1.07 °C in summertime and 1.53 °C in wintertime. Considering the average minimum temperatures, these difference between urban and rural context increase up to 2.60 °C and 2.46 °C respectively in summertime and wintertime.

In Table 7 also the heatwave and the cold-wave on the years 2010-2016 have been evaluated; the heatwaves as events with the average and the maximum temperature over the 97.5[th] percentile and cold-waves as events with the average and the minimum temperature under the 2.5[th] percentile [25].

Table 7. The UHI effects.

Weather station	Inh/km²	Spring/summer months [°C]					Autumn/winter months [°C]					Heatwave °C		Cold wave °C	
		Tm	Tmax	Tmin	Q1	Q2	Tm	Tmax	Tmin	Q1	Q2	Tavg	Tmax	Tavg	Tmin
URBAN WEATHER STATIONS															
Via della Consolata	86,410	21.15	26.20	16.62	5.04	9.58	8.14	12.33	4.70	4.19	7.63	28.00	33.7	1.4	-1.3
Politecnico	86,272	21.41	25.88	19.31	4.42	8.57	8.52	12.42	5.17	3.90	7.25	28.35	33.2	1.6	-1.3
Reiss Romoli	17,218	20.47	25.87	15.45	5.40	10.42	7.41	12.12	3.42	4.70	8.70	27.20	33.1	0.5	-3.0
Alenia	16,181	20.28	25.75	15.32	5.47	10.43	7.34	11.82	3.52	4.48	8.30	27.10	33.2	0.5	-2.9
INRIM	15,659	20.38	25.88	14.98	5.51	10.90	6.49	11.35	2.30	4.86	9.05	26.11	33.5	0.1	-4.1
RURAL WEATHER STATIONS															
Vallere	13,701	19.95	26.32	14.42	6.36	11.88	6.32	11.79	2.12	5.47	9.67	26.60	33.8	-0.6	-4.2
Rivoli La Perosa	6,616	20.08	26.45	14.36	6.37	12.09	6.61	12.20	1.83	5.59	10.37	27.00	34.1	-0.2	-5.1
Caselle	2,669	19.95	26.01	14.08	6.08	11.94	6.40	12.11	1.59	5.70	10.49	26.70	33.3	-0.5	-5.4
Brandizzo	3,125	19.63	25.82	13.98	6.18	11.84	5.97	11.44	1.51	5.48	9.92	26.20	33.1	-0.7	-5.1
Bauducchi	667	19.81	27.15	13.18	7.34	13.98	5.74	11.97	1.03	6.23	10.94	26.30	34.6	-1.1	-5.5
Venaria La Mandria	685	18.91	25.99	12.63	7.03	13.36	5.45	11.97	0.38	6.52	11.60	25.70	33.5	-1.4	-6.5
Venaria Ceronda	8,555	19.33	25.56	13.50	6.22	12.07	5.84	11.86	1.09	6.02	10.77	25.90	32.8	-0.9	-5.7

6. DISCUSSION

The best results, with lower percentages of relative error between measured and calculated air temperatures, were provided with equations 8 and 13 including all the variables (even if the errors are very similar). Not always, it is possible to have the data of all the environmental variables for each portion of the territory and therefore it is sometimes necessary to use alternative models with relative errors however low. In addition, the correctness of the databases is fundamental to identify a model, especially on such a large scale.

With equations 8 and 13, the most influential variables were BCR, MOS, and H_2O with both Landsat and the Aster satellite data (see Figure 11). The influence of the different variables is highlighted, so it is the built environment that most influences air temperature variations. A good urban planning can help in mitigating the global warming and the UHI effects. A more accurate knowledge of urban areas with a detailed map of urban variables can allow the optimization of interventions using these models with a compensative approach.
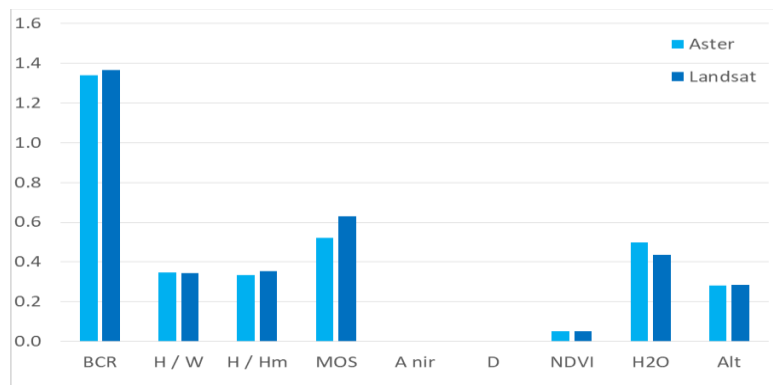
Figure 11. The range of variability of the different variables multiplied by the coefficients α (on the air temperature) with equations 8 and 13.

The average relative difference between the LST and the air temperature is 3% with Aster satellite data. In the suburban context, due to the presence of vegetation, the difference between these temperatures could be of 1%, while in the urban context the percentage rises up to 8% for the presence of high emissivity materials and for the presence of the UHI. Higher values can be found with Landsat images that have a lower resolution but the results were acceptable.

The UHI effects are influenced by the built density (i.e. BCR in Figure 9) and then by the people density, as also reported in Table 7. From this analysis, the land-cover-driven indicator Q3 seems to better explain the UHI effects then the UHI-driven indicators Q1 and Q2, which were influenced by the higher average temperature in the urban contexts.

The results of this analysis can be improved with the hourly data instead the daily average, maximum and minimum weather data.

7. CONCLUSIONS

A simple linear regression could evaluate with a good accuracy the effect of territorial variables on the microclimate variations and the UHI effect. At the

same time, a simple model like this one can be used to plan and design a more sustainable built environment as a function of the urban and territorial variables. The presence of vegetation and water, for example, can reduce the air temperatures up to -0.5 °C on the average daily temperature (see Figure 11).

Better results can be obtained from the most accurate models that describe the environment with a greater number of variables and the support of a GIS tool can certainly optimize this representation. In this work, all the linear regression models have a relative error lower that 10 %.

With this methodology, also the UHI effect can be evaluated and, for the Metropolitan City of Turin, it was quantified with the land cover-driven indicator "urban-rural" Q3 measured with the difference of the daily air temperature between urban and rural areas. The results are of 1-1.5 °C with the average air temperatures respectively in summertime and wintertime; and of 2.6-2.46 °C with the minimum air temperatures respectively in summertime and wintertime. Also, the UHI-driven indicators Q1 and Q2 can be used to evaluate the UHI intensity even if, with the daily temperatures, they are influenced by the higher urban temperatures. In this analysis, the effect of the UHI are more evident in wintertime as also demonstrated with the heatwaves and cold-waves data.

Future researches with hourly weather data could improve these models.

8. ACKNOWLEDGEMENTS

9. REFERENCES

[1] Lamarca C., Qüense J., Henríquez C., "Thermal comfort and urban canyons morphology in coastal temperate climate, Concepción, Chile", *Urban Climate*, 2016.

[2] van Hove L. W. A., Jacobs C. M. J., Heusinkveld B. G., Elbers J. A., van Driel B. L., Holtslag A. A. M., "Temporal and spatial variability of urban heat island and thermal comfort within the Rotterdam agglomeration", *Building and Environment*, **vol. 83**, pp. 91-103, 2015.

[3] Schwarz N., Lautenbach S., Seppelt R., "Exploring indicators for quantifying surface urban heat islands of European cities with MODIS land surface temperatures", *Remote Sensing of Environment*, **vol. 115**, (issue no. 12), pp. 3175-3186, 2011.

[4] Mirzaei P. A., "Recent challenges in modeling of urban heat island", *Sustainable Cities and Society*, **vol. 19**, pp. 200-206, 2015.

[5] Bakarman M. A., Chang J. D., "The Influence of Height/width Ratio on Urban Heat Island in Hot-arid Climates", *Procedia Engineering*, **vol. 118**, pp. 101-108, 2015.

[6] Yang J., Wang Z., Kaloush K. E., "Environmental impacts of reflective materials: Is high albedo a 'silver bullet' for mitigating urban heat island?", *Renewable and Sustainable Energy Reviews*, **vol. 47**, pp. 830-843, 2015.

[7] Mutani G., "Urban planning for the liveability and thermal comfort of outdoor spaces", 11th Conference on Sustainable of Energy, Water and Environmental Systems, Lisbon, 2016.

[8] Mazzotta A., Mutani G., "Environmental High Performance Urban Open Spaces Paving: Experimentations in Urban Barriera (Turin, Italy)", *Energy Procedia*, **vol. 78**, pp. 669-674, 2015.

[9] Coseo P., Larsen L., "Cooling the Heat Island in Compact Urban Environments: The Effectiveness of Chicago's Green Alley Program", *Procedia Engineering*, **vol. 118**, pp. 691-710, 2015.

[10] Delmastro C., Mutani G., Pastorelli M., Vicentini G., Urban morphology and energy consumption in Italian residential buildings, *4th International Conference on Renewable Energy Research and Applications ICRERA 2015*, IEEE Conference Publications, pp. 1603-1608, 2015.

[11] Ceretti G., Turin and the urban heat island. A model for a sustainable urban planning, *Master Thesis in Sustainable Architecture*, Supervisor Mutani G., Politecnico di Torino, 2015.

[12] Mutani G., Fiermonte F., "The Urban Microclimate and the Urban Heat Island. A model for a sustainable urban planning", *Urban and Landscape Perspectives*, Springer International Publishing, 2016.

[13] Weng Q., Lu D., Schubring J., "Estimation of land surface temperature–vegetation abundance relationship for urban heat island studies", *Remote Sensing of Environment*, **vol. 89**, (issue no. 4), pp. 467-483, 2004.

[14] Zhang H., Qi Z., Ye X., Cai Y., Ma W., Chen M., "Analysis of land use/land cover change, population shift, and their effects on spatiotemporal patterns of urban heat islands in metropolitan Shangai, China", *Applied Geography*, **vol. 44**, pp. 121-133, 2013.

[15] Stathopoulou M., Cartalis C., "Downscaling AVHRR land surface temperatures for improved surface urban heat island intensity estimation", Remote Sensing of Environment, **vol. 113**, (issue no. 12), pp. 2592-2605, 2009.

[16] Mills G et al., "Climate Information for Improved Planning and Management of Mega Cities (Needs Perspective)", Procedia Environmental Sciences, **vol. 1**, pp. 228-246, 2010.

[17] Cui Y., Yan D., Hong T., Ma J., "Temporal and spatial characteristics of the urban heat island in Beijing and the impact on building design and energy performance", *Energy*, **vol. 130**, pp. 286-297, 2017.

[18] Jusuf S. K., Wong N. H., Hagen E., Anggoro R., Hong Y., "The influence of land use on the urban heat island in Singapore", *Habitat International*, **vol. 31**, no. 2, pp. 232-242, 2007.

[19] Middel A., Häb K., Brazel A. J., Martin C. A., Guhathakurta S., "Impact of urban form and design on mid-afternoon microclimate in Phoenix Local Climate Zones", *Landscape and Urban Planning*, **vol. 122**, pp. 16-28, 2014.

[20] Palme M., Inostroza L., Villacreses G., Lobato-Cordero A., Carrasco C., "From urban climate to energy consumption. Enhancing building performance simulation by including the urban heat island effect", *Energy and Buildings*, **vol. 145**, pp. 107-120, 2017.

[21] Pyrgou A., Castaldo V.L., Pisello A.L., Cotana F., Santamouris M., "Differentiating responses of weather files and local climate change to explain variations in building thermal-energy performance simulations", *Solar Energy*, **vol. 153**, pp.224–237, 2017.

[22] Morabito M., Crisci A., Gioli B., Gualtieri G., Toscano P., Di Stefano V., Orlandini S., Gensini G.F., "Urban-Hazard Risk Analysis: Mapping of Heat-Related Risks in the Elderly in Major Italian Cities", *PLoS ONE*, **vol.10 (5)**, doi:10.1371/journal.pone.0127277, pp.1-18, 2015.

[23] Vuckovic M., Kiesel K., Mahdavi A., "Toward advanced representation of the urban microclimate in building performance simulation", *Sustainable Cities and Society*, **vol. 27**, pp. 356-366, 2016.

[24] Thomas G., Sherin A. P., Ansar S., Zachariah E. J., "Analysis of Urban Heat Island in Kochi, India, Using a Modified Local Climate Zone Classification", *Procedia Environmental Sciences*, **vol. 21**, pp. 3-13, 2014.

[25] Pyrgou A., Castaldo V. L., Pisello A. L., Cotana F., Santamouris M., "Differentiating responses of weather files and local climate change to explain variations in building thermal-energy performance simulations", *Solar Energy*, **vol. 153**, pp. 224-237, 2017.

[26] Shi T., Huang Y., Wang H., Shi C., Yang Y., "Influence of urbanization on the thermal environment of meteorological station: Satellite-observed evidence", *Advances in Climate Change Research*, **vol. 6**, (issue no. 1), pp. 7-15, 2015.

[27] Sharmin T., Steemers K., "Responsiveness of microclimate simulation tool in recognising diversity in urban geometry", *Cities, Buildings People: Toward Regenerative Environments*, **vol. 1**, pp. 2-9, 2016.

[28] Liang S., "Narrowband to broadband conversions of land surface albedo: I. Algorithms", Remote Sensing of Environment, **vol. 76**, pp. 213-238, 2000.

[29] Liang S. et al., "Narrowband to broadband conversions of land surface albedo: II. Validation", Remote Sensing of Environment, **vol. 84**, pp. 25-41, 2002.

[30] Lelovics E., Pongrácz R., Bartholy J., "Satellite- and Ground-Based Temperature Observations used in Assessing the Urban Heat Island Phenomena", *Procedia Computer Science*, **vol. 7**, pp. 183-184, 2011.

[31] Sheng L., Tang X., You H., Gu Q., Hu H., "Comparison of the urban heat island intensity quantified by using air temperature and Landsat land surface temperature in Hangzhou, China", Ecological Indicators, **vol. 72**, pp. 738-746, 2017.